

# A numerical test of the Y-system in the small size limit of the $SU(2) \times SU(2)$ Principal Chiral Model

---

**Matteo Beccaria and Guido Macorini**

*Dipartimento di Fisica, Universita' del Salento, Via Arnesano, 73100 Lecce*

*INFN, Sezione di Lecce*

*E-mail: [matteo.beccaria@le.infn.it](mailto:matteo.beccaria@le.infn.it), [guido.macorini@le.infn.it](mailto:guido.macorini@le.infn.it)*

**ABSTRACT:** Recently, Kazakov, Gromov and Vieira applied the discrete Hirota dynamics to study the finite size spectra of integrable two dimensional quantum field theories. The method has been tested from large values of the size  $L$  down to moderate values using the  $SU(2) \times SU(2)$  principal chiral model as a theoretical laboratory. We continue the numerical analysis of the proposed non-linear integral equations showing that the deep ultraviolet region  $L \rightarrow 0$  is numerically accessible. To this aim, we introduce a relaxed iterative algorithm for the numerical computation of the low-lying part of the spectrum in the  $U(1)$  sector. We discuss in details the systematic errors involved in the computation. When a comparison is possible, full agreement is found with previous TBA computations.

---

## Contents

<b>1. Introduction</b>	<b>1</b>
<b>2. Y-system equations</b>	<b>3</b>
2.1 A second formula for the ground state energy	6
<b>3. Numerical implementation</b>	<b>6</b>
3.1 Discretization	6
3.2 Fixed point search	7
3.3 Algorithm for the excited state $\Theta_0$	8
3.4 Algorithm for the excited state $\Theta_{00}$	8
3.5 Alternative algorithm for the ground state	9
<b>4. Numerical Results</b>	<b>9</b>
4.1 Ground State	10
4.2 First excited state $\Theta_0$	10
4.3 Excited state $\Theta_{00}$	11
4.4 Summary tables and $L \rightarrow 0$ limit	11
<b>5. Conclusions</b>	<b>12</b>

---

## 1. Introduction

Finite size corrections to the complete spectrum of quantum field theories are an important issue with many applications. In particular, they are relevant to the aim of testing Maldacena's AdS/CFT duality relating type IIB superstring propagating in  $AdS_5 \times S^5$  and  $\mathcal{N} = 4$  SYM [1]. In the 't Hooft planar limit, the gauge theory composite operators have anomalous dimensions related to the spectrum of a finite size integrable super spin chain [2]. The so-called *wrapping* corrections are crucial to check the correspondence and have been the subject of major investigations in recent years [3].

As shown by Lüscher [4], the leading corrections to the mass gap in rather general relativistic models can be computed in terms of their infinite size scattering matrix. In integrable models, the  $S$ -matrix is one of the central objects and is known exactly. This suggests that the complete size corrections can be in reach. Indeed, for continuum models admitting an integrable discretization, it is possible to determine the spectrum of all states by solving the associated (nested) Bethe Ansatz equations. Their continuum limit leads to the Destri-de Vega non-linear integral equations (DdV NLIE) [5]. When an integrable discretization is not available, it is possible to determine the finite size correction to the

ground state energy by means of the thermodynamical Bethe Ansatz (TBA) [6, 7, 8]. The general idea is that, in relativistic (Euclidean) 2d models, the free energy is related to the ground state energy in finite volume by a modular transformation exchanging spatial extension and inverse temperature. Usually, the method leads to an infinite system of coupled non linear integral equations which can be rewritten in the functional Y-system form which is universal, *i.e.* symmetry based [9].

Apparently, the very nature of the TBA construction forbids the computation of excited energies. Nevertheless, various extensions have been proposed [6]. Indeed, there are cases under full control, like for instance the Sine-Gordon model [8], where the very same Y-system form of the TBA describes excited states. They are associated to solutions of the Y-system with different boundary conditions and analytical properties. Due to this important remark, the Y-system is the most promising object for the study of the full spectrum.

In the AdS/CFT case, duality with string theory plays a crucial role by mapping the discrete spin chain describing finite length operators to states of a continuum  $\sigma$ -model. In the end, it allows to apply the general idea of TBA and to obtain the remarkable formulations described in [10]<sup>1</sup>. The resulting Y-system leads to a very involved set of coupled non-linear integral equations where numerical methods are welcome, if not mandatory.

Here, we begin a systematic investigation of such numerical algorithms by going back to the initial analysis of Kazakov, Gromov and Vieira who choose the Principal Chiral Model (PCM) as a theoretical laboratory. In [11], the authors (GKV) assume that the Y-system provides a complete description of the full spectrum provided suitable solutions are considered. GKV describe a new systematic way to deal with the infinite component Y-system. They stress the important fact that the Y-system is closely related to the Hirota bilinear equation [9]. For finite rank symmetry group of the integrable model, the Hirota dynamics can be solved in terms of a finite number of functions of the spectral parameter. Thus, the Y-system is successfully reduced to a finite system of non-linear integral equations (NLIE) rather suitable for numerical methods.

In the GKV analysis, the proposed method is partially tested on the  $SU(2) \times SU(2)$  Principal Chiral Model (PCM), equivalent to the  $O(4)$   $\sigma$ -model. Measuring all dimensional quantities in terms of the mass gap, the only parameter which describes the spectrum is the continuous system size  $L$ . The low-lying part of the spectrum (including the ground state energy) is computed for  $10^{-1} \leq L \leq 2$  by a numerical iterative algorithm. The general strategy starts from an approximate solution to the NLIE at large  $L$ . Then, the numerical solution is found by iteration of the NLIE and the size  $L$  is progressively reduced down to the desired value. The ground state and the first excited state energies can be compared with [7] where they are computed by means of coupled DdV-like equations, apparently unrelated to the GKV NLIE<sup>2</sup>. The agreement is good and reasonably

---

<sup>1</sup>Actually, the string is quantized in light-cone gauge which means that relativistic invariance is broken. This requires to compute the free energy of a mirror model which is not the same as the original theory.

<sup>2</sup>Although, *a priori*, it is not excluded that the two formulations can be related by some change of variable.

compatible with the expected behaviour in the deep ultraviolet region  $L \ll 1$  which however remains unexplored at the smallest considered size,  $L = 0.1$ . In a subsequent paper, the analysis of [11] has been extended to the  $SU(N) \times SU(N)$  PCM [12]. For  $N = 3$ , the spectrum of various excitations is extracted as a function of the size  $L$  down to  $L = 10^{-3}$ . Unfortunately, for  $N = 4$  already  $L \sim 1$  is not accessible due to instabilities in the iterative solution of the NLIE.

In this paper, we reconsider the GKV integral equations for the  $N = 2$  model going down to very small size values providing a definitive test of their validity, at least in this region. We accomplish this task by a numerical analysis and present some refinements of the numerical strategy which, in principle, could be useful for the study of  $N > 2$  models. In particular we adopt a straight discretization of the NLIE which allows for a very clean control of the systematic errors. Also, we improve the iteration procedure by introducing various relaxation parameters turning out to be crucial in order to reach  $L = 10^{-8}$ . These very small values of the size are even smaller than those achieved in previous studies of the deep UV region where a comparison with asymptotically free field theory is possible [7, 8, 13]. The outcome of our analysis is a very good agreement between the GKV equations and other known results. Besides, our numerical implementation is very simple and easily under control.

The plan of the paper is the following. In Sec. (2), we briefly summarize the GKV approach and its associated NLIEs. In Sec. (3), we describe our numerical algorithms for the ground state and two excited states of interest. Finally, in Sec. (4), we discuss the numerical results with particular attention to the role of systematic errors and relaxation parameters.

## 2. Y-system equations

In this section we briefly summarize the NLIE that we are going to solve numerically. They are derived in full details in [11]. Here we just sketch the main ideas and introduce the necessary quantities.

The  $SU(2) \times SU(2)$  Principal Chiral Model, equivalent to the  $O(4)$   $\sigma$ -model, is described by the action

$$S = -\frac{1}{2e_0^2} \int d^2x \operatorname{Tr} \left( h^{-1} \partial_a h \right)^2, \quad h \in SU(2). \quad (2.1)$$

This model is asymptotically free. The infinite size spectrum contains a single physical particle with a dynamically generated mass  $m = \Lambda_{UV} e^{\frac{-2\pi}{e_0^2}}$ ,  $\Lambda_{UV}$  being the ultraviolet cut-off. The associated state transforms in the bifundamental of  $SU(2) \times SU(2)$ . The elastic scattering matrix is known and can be written in terms of the scalar factor [15]

$$S_0(\theta) = i \frac{\Gamma\left(\frac{1}{2} - \frac{i\theta}{2}\right) \Gamma\left(\frac{i\theta}{2}\right)}{\Gamma\left(\frac{1}{2} + \frac{i\theta}{2}\right) \Gamma\left(-\frac{i\theta}{2}\right)}. \quad (2.2)$$

In general, one can consider states with  $N$  particles and polarization defined by the number of left and right spins down<sup>3</sup>. In this paper we shall consider the so-called  $U(1)$  sector where all spins are up (ferromagnetic polarization). The infinite size energy of such states can be computed from the formula

$$E = m \sum_{i=1}^N \cosh(\pi \theta_i), \quad (2.3)$$

where the physical rapidities  $\{\theta_i\}_{i=1,\dots,N}$  solve the asymptotic Bethe Ansatz [14]

$$e^{-iL \sinh(\pi \theta_i)} = - \prod_{j=1}^N S_0^2(\theta_i - \theta_j). \quad (2.4)$$

In the TBA approach, the finite size ground state energy is computed starting from the infinite size thermodynamics associated to the above equations. If we denote by  $L$  the size in units of the mass gap, then the result is the following simple formula for the energy

$$E_0(L) = -\frac{1}{2} \int_{\mathbb{R}} d\theta \cosh(\pi \theta) \log(1 + Y_0), \quad (2.5)$$

where  $Y_0$  is obtained from the solution of the TBA equations. These are integral equations which, upon reasonable physical assumptions, can be written in the celebrated  $Y$ -system form<sup>4</sup>

$$Y_n^+ Y_n^- = (1 + Y_{n-1})(1 + Y_{n+1}), \quad n \in \mathbb{Z}. \quad (2.6)$$

The physical boundary conditions predict the large  $\theta$  behaviour of  $Y_n$ . All  $Y_n$  with  $n \neq 0$  tend to a constant, while  $Y_0$  is exponentially suppressed according to

$$Y_0(\theta) \sim e^{-L \cosh(\pi \theta)}. \quad (2.7)$$

As we explained in the introduction, the central problem is that of solving the  $Y$ -system since the main assumption is that it describes all states and not only the ground state.

The GKV method to study Eq. (2.6) is based on the relation to the Hirota equation that can be written as ( $\bar{\Phi}$  is the conjugate of  $\Phi$ )

$$T_n \left( \theta + \frac{i}{2} \right) T_n \left( \theta - \frac{i}{2} \right) - T_{n-1}(\theta) T_{n+1}(\theta) = \Phi \left( \theta + \frac{in}{2} \right) \bar{\Phi} \left( \theta - \frac{in}{2} \right), \quad (2.8)$$

where the functions  $T_n$  are related to  $Y_n$  by the relation

$$Y_n(\theta) = \frac{T_{n+1}(\theta) T_{n-1}(\theta)}{\Phi \left( \theta + \frac{in}{2} \right) \bar{\Phi} \left( \theta - \frac{in}{2} \right)} = \frac{T_n \left( \theta + \frac{i}{2} \right) T_n \left( \theta - \frac{i}{2} \right)}{\Phi \left( \theta + \frac{in}{2} \right) \bar{\Phi} \left( \theta - \frac{in}{2} \right)} - 1. \quad (2.9)$$

Eqs. (2.8, 2.9) are gauge invariant according to

$$Y_n(\theta) \longrightarrow Y_n(\theta),$$

---

<sup>3</sup>Here, left and right refer to the two  $SU(2)$  factors, or wings.

<sup>4</sup>The notation is  $f^{\pm \dots \pm}(x) = f(x \pm \frac{i}{2})$ , when we have  $p$  plus or minus signs.

$$\begin{aligned}
T_n(\theta) &\longrightarrow g\left(\theta + \frac{in}{2}\right) \bar{g}\left(\theta - \frac{in}{2}\right) T_n(\theta), \\
\Phi(\theta) &\longrightarrow g\left(\theta - \frac{i}{2}\right) g\left(\theta + \frac{i}{2}\right) \Phi(\theta).
\end{aligned}
\tag{2.10}$$

The Hirota equation is integrable (it admits a discrete Lax pair) and this allows for a complete analysis of its solutions [11].

The main trick of GKV is a clever continuation from the case of large  $L$  where a fundamental important simplification occurs. Indeed, the  $L \rightarrow \infty$  suppression of  $Y_0$  leads to a decoupling of the  $Y$ -system in the two sets  $\{Y_n\}$  with  $n > 0$  or  $n < 0$ . Both can be written, according to (2.9), in terms of a suitable solution of the Hirota equation and thus we identify two independent solutions of it. This picture can be continued to finite  $L$  as carefully shown in [11]. The resulting two independent solutions are no more decoupled and give nontrivial  $T_n$  for all  $n$  on both wings of the  $SU(2) \times SU(2)$  Dynkin diagram. These two solutions describe the same state and must be related by a gauge transformation  $g(\theta)$ . This consistency condition gives a single NLIE for the function  $g$  which is precisely the equation we are going to study. Once this equation is solved, the function  $Y_0$  associated to the desired excited states is available, and the formula for the energy simply becomes

$$E(L) = m \sum_{i=1}^N \cosh(\pi \theta_i) - \frac{1}{2} \int_{\mathbb{R}} d\theta \cosh(\pi \theta) \log(1 + Y_0). \tag{2.11}$$

Let us introduce the definitions

$$A(\theta) = (g^+(\theta))^2, \quad K_0(\theta) = \frac{1}{2\pi i} \frac{d}{d\theta} \log S_0^2(\theta). \tag{2.12}$$

The function  $A(\theta)$  is determined by the NLIE [11] (a star denotes as usual convolution with respect to the rapidity argument)

$$A = -e^{-L \cosh(\pi \theta)} \prod_{i=1}^N S_0^2\left(\theta - \theta_i + \frac{i}{2}\right) \exp\left(K_0 * \log \frac{A-1}{|A|-1} - K_0^{++} * \log \frac{\bar{A}-1}{|\bar{A}|-1} - \log \frac{\bar{A}-1}{|\bar{A}|-1}\right), \tag{2.13}$$

where the physical rapidities are self consistently determined by

$$-e^{iL \sinh(\pi \theta_i)} \prod_{j=1}^N S_0^2(\theta_i - \theta_j) \exp\left[2i \operatorname{Im}\left(K_0^- * \log \frac{A-1}{|A|-1}\right)\right]_{\theta=\theta_i} = 1. \tag{2.14}$$

According to Eq. (2.11), the energy is given by

$$E(L) = \sum_{i=1}^N \cosh(\pi \theta_i) - \int_{\mathbb{R}} d\theta \cosh(\pi \theta) \log \frac{A-1}{|A|-1}. \tag{2.15}$$

This formula can also be used for the ground state which is associated with  $N = 0$ . In this case, all factors  $S_0$  must be replaced by 1, leaving of course the kernel  $K_0$  untouched.

## 2.1 A second formula for the ground state energy

Remarkably, an alternative NLIE for the ground state energy is also presented in [11]. It is a self-consistent equation for the function  $f(\theta)$  which reads <sup>5</sup>

$$f(\theta) = 2 T_1(\theta) \left| T_0 \left( \theta + \frac{i}{2} + i 0 \right) \right|^2 \exp \left[ -L \cosh(\pi \theta) - 2s * \log |T_0^{++}|^2 \right], \quad (2.17)$$

where  $T_n$  are obtained from  $f$  according to

$$T_{n-1} = n + \frac{n}{\pi(4\theta^2 + n^2)} * f, \quad (2.18)$$

and where the function  $s(\theta)$  is

$$s(\theta) = \frac{1}{2 \cosh(\pi \theta)}. \quad (2.19)$$

Once Eq. (2.17) is solved, the energy is given by (2.5) with the following expressions for  $Y_0$

$$Y_0 = \frac{T_1(\theta) f(\theta)}{2 \left| T_0 \left( \theta + \frac{i}{2} + i 0 \right) \right|^2} \quad (2.20)$$

We shall discuss the numerical accuracy and efficiency of this second approach comparing it with the general formula for  $N$  particle states specialized at  $N = 0$ .

## 3. Numerical implementation

### 3.1 Discretization

A numerical implementation of Eqs. (2.13, 2.14) has been presented in [11] in terms of a short Mathematica code exploiting various high level functions for numerical integration and interpolation. Instead, our approach will be that of presenting a simple algorithm which can kept easily under control in order to check the continuum limit and the bias due to systematic errors. To this aim we cut-off the rapidity  $\theta$  in the interval  $|\theta| \leq \Lambda$  and split it introducing the discrete points

$$\theta_n = \Lambda \left( -1 + 2 \frac{n-1}{M-1} \right) \equiv \Lambda \xi_n, \quad n = 1, \dots, M. \quad (3.1)$$

For numerical efficiency, we define the fixed vectors and matrices

$$\begin{aligned} Z_n^{(1)} &= -e^{-L \cosh(\pi \theta_n)} S_0 \left( \theta_n + \frac{i}{2} \right)^2, \quad n = 1, \dots, M, \\ \tilde{Z}_n^{(2)} &= \begin{cases} \frac{2 \log 2}{\pi}, & n = 0, \\ K_0 \left( \frac{2 n \Lambda}{M-2} \right), & n \neq 0, \end{cases} \quad n = -M, \dots, M, \end{aligned} \quad (3.2)$$

---

<sup>5</sup>Note that the singular convolution is more explicitly

$$\frac{1}{\pi} \int_{\mathbb{R}} d\xi \frac{1}{4(\theta - \xi + \frac{i}{2} + i 0)^2 + 1} f(\xi) = \frac{1}{\pi} \oint_{\mathbb{R}} d\xi \frac{1}{4(\theta - \xi + \frac{i}{2})^2 + 1} f(\xi) - \frac{1}{4} f(\theta). \quad (2.16)$$

$$\begin{aligned}
\tilde{Z}_n^{(3)} &= \begin{cases} 0, & n = 0, \\ K_0 \left( \frac{2n\Lambda}{M-2} + i \right) & n \neq 0, \end{cases} & n = -M, \dots, M, \\
Z_{nm}^{(2)} &= \tilde{Z}_{n-m+M+1}^{(2)}, & n, m = 1, \dots, M, \\
Z_{nm}^{(3)} &= \tilde{Z}_{n-m+M+1}^{(3)}, & n, m = 1, \dots, M,
\end{aligned}$$

They are evaluated with a (large) fixed number of digits of order 200. The issue of numerical precision will be discussed later. We now present the numerical algorithms for the ground state, the first excited state which has a zero Bethe root, and another state which is non trivial from the Bethe Ansatz point of view having two opposite Bethe roots.

### 3.2 Fixed point search

The NLIE that we want to solve takes the form of a fixed point equation  $f(x) = x$ . It can be solved by iteration when the map  $x \mapsto f(x)$  is a contraction. In other words, one simply sets  $x_{n+1} = f(x_n)$  and the sequence  $\{x_n\}$  converges to the solution  $x^*$  as  $n \rightarrow \infty$ , independent on the starting point. In actual cases, one needs to start in a suitable small neighborhood of  $x^*$ . Then, the map can be linearized in terms of the small differences  $\delta_n = x_n - x^*$  and one has to iterate

$$\delta_{n+1} = a \delta_n, \quad a \equiv f'(x^*). \quad (3.3)$$

Convergence is exponentially good for  $|a| < 1$ , otherwise the sequence diverges. Following Jacobi and Seidel, a simple general trick to deal with the case  $|a| > 1$  is to introduce a relaxation parameter and consider some average between the old and new values of the  $\delta$  variables. In other words, one considers the following modified equation

$$x_{n+1} = (1 - \lambda) x_n + \lambda f(x_n), \quad (3.4)$$

where  $\lambda$  is a real number. The advantage is clear. Around the fixed point one has

$$\delta_{n+1} = (1 - \lambda + \lambda a) \delta_n. \quad (3.5)$$

This means that in the unstable case,  $|a| > 1$ , we can enforce stability by simply choosing

$$\begin{cases} a > 1 & : -\frac{2}{a-1} < \lambda < 0, \\ a < -1 & : 0 < \lambda < \frac{2}{1-a}, \end{cases} \quad (3.6)$$

In the  $p$ -component case, where  $x_n \in \mathbb{C}^p$ , the same argument based on the linearization around the fixed point, suggest to replace  $\lambda$  by a  $p \times p$  matrix and to apply (3.6) to each eigenvalue of the matrix  $\nabla f$ . More involved schemes can be devised replacing (3.5) by higher order relaxation processes as in the inertial relaxation discussed in [16] or also finding adaptive algorithms for the step by step choice of  $\lambda$  [17]. In this paper, we shall discuss the simplest implementation of the relaxation idea as illustrated above.



### 3.3 Algorithm for the excited state $\Theta_0$

Let us begin our discussion with the 1-particle state  $\Theta_0$ . It is discussed in [11] and is the lightest excited state. So, it enters the mass gap computation. By symmetry, there is only one Bethe roots which is fixed at zero. This simplifies a lot the computation.

The function  $A(\theta)$  becomes a sequence of vectors  $\{A_n^{(k)}\}_{k \geq 0, 1 \leq n \leq M}$  which takes the initial value

$$A_n^{(0)} = Z_n^{(1)} = -e^{-L \cosh(\pi \theta_n)} S_0 \left( \theta_n + \frac{i}{2} \right)^2. \quad (3.7)$$

Then, the main loop starts. Defining

$$r_n^{(k)} = \log \frac{A_n^{(k)} - 1}{|A_n^{(k)}| - 1}, \quad (3.8)$$

we have

$$A_n^{(k)} = (1 - \lambda) A_n^{(k-1)} + \lambda Z_n^{(1)} \exp \left[ \frac{2\Lambda}{M-2} \sum_{m=1}^N w_m \left( Z_{nm}^{(2)} r_m^{(k-1)} - Z_{nm}^{(3)} \bar{r}_m^{(k-1)} \right) - \bar{r}_n^{(k-1)} \right]. \quad (3.9)$$

The parameter  $\lambda$  is a relaxation parameter introduced according to the previous discussion. It is crucial at small  $L$  as we shall discuss. The algorithm in [11] is obtained for  $\lambda = 1$  and works for  $L$  of order  $10^{-1}$ . We shall push the computation several orders of magnitude beyond this value. In this deep UV region, the above map is no more a contraction and convergence is lost. Nevertheless, a moderate value of  $\lambda \in (0, 1)$ <sup>6</sup> will turn out to be enough to restore convergence. The weights  $w_m$  are used to approximate integrations by summations. They can be taken at the rough value  $w_m \equiv 1$  or improved as in Simpson or higher order integrations. For our purposes this is not a crucial issue as we shall explain later.

The very same algorithm can be applied to the ground state. The only necessary change is the replacement of all  $S_0$  factors by unity. In conclusion the parameters entering the numerical algorithm are

$$\Lambda, \quad M, \quad \lambda. \quad (3.10)$$

### 3.4 Algorithm for the excited state $\Theta_{00}$

This is a 2-particle state. By symmetry, it is associated with a pair of opposite rapidities  $\pm\theta^*$  solving the Bethe Ansatz equations. Again, we start from the method presented in [11], but add the important relaxation parameters. Indeed, it is convenient to choose two independent relaxation times for the function  $A$  and for the Bethe root(s). This is a fundamental point otherwise convergence is soon lost.

---

<sup>6</sup>We never observed the necessity of over-relaxation.

Let us denote by  $\{\tilde{\theta}_a^{(k)}\}_{a=1,2}$ , with  $\tilde{\theta}_2^{(k)} = -\tilde{\theta}_1^{(k)}$ , the two Bethe rapidities. They satisfy the BA equations (actually it is one equation due to the parity symmetry !) [11],

$$L \sinh(\pi \tilde{\theta}_a^{(k)}) - i \sum_{\substack{a \neq b \\ b=1}}^2 \log S_0(\tilde{\theta}_a^{(k)} - \tilde{\theta}_b^{(k)})^2 + \frac{4\Lambda}{M-2} \sum_{\ell=1}^M \text{Im} \left( K_0 \left( \tilde{\theta}_a^{(k-1)} - \theta_\ell - \frac{i}{2} \right) r_\ell^{(k-1)} \right) = 0. \quad (3.11)$$

The initial value of the Bethe roots is not critical and a possible choice is just to solve the above equation suppressing the last term in the left hand side. The modified main loop is then

$$\begin{aligned} A_n^{(k)} = & (1 - \lambda_1) A_n^{(k-1)} + \\ & + \lambda_1 Z_n^{(1)} \prod_{a=1}^2 S_0(\theta_n - \tilde{\theta}_a^{(k-1)} + \frac{i}{2})^2 \times \\ & \times \exp \left[ \frac{2\Lambda}{M-2} \sum_{m=1}^N w_m \left( Z_{nm}^{(2)} r_m^{(k-1)} - Z_{nm}^{(3)} \bar{r}_m^{(k-1)} \right) - \bar{r}_n^{(k-1)} \right]. \end{aligned} \quad (3.12)$$

In addition, we must provide an update rule for the Bethe roots. We propose

$$\tilde{\theta}_a^{(k)} = (1 - \lambda_2) \tilde{\theta}_a^{(k-1)} + \lambda_2 \tilde{\theta}_a^{(k-1)}. \quad (3.13)$$

In summary, the parameters entering the numerical algorithm are

$$\Lambda, \quad M, \quad \lambda_1, \quad \lambda_2. \quad (3.14)$$

As a remark, we note that for more complicated states with more Bethe roots, we still have two relaxation parameters, one for the function  $A$  and one for the Bethe roots.

### 3.5 Alternative algorithm for the ground state

The numerical implementation of the solution of (2.17) is completely analogous to that described in Sec. (3.3). The initial value of the discretized  $f$  function is

$$f_n^{(0)} = 4 e^{-L \cosh(\pi \theta_n)}. \quad (3.15)$$

## 4. Numerical Results

We present here our numerical results aimed at understanding (a) the systematic errors associated with finite values of  $\Lambda$ ,  $M$ , (b) the role of the relaxation parameters  $\lambda_i$ . Let us begin with the cut-off  $\Lambda$ . In principle, one should consider a fixed  $\Lambda$  and send  $M \rightarrow \infty$  in order to reach the continuum limit. The result is a function of  $\Lambda$  which has to be extrapolated at  $\Lambda \rightarrow \infty$ . In practice, as soon as  $\Lambda$  is large enough to cover the support of the function  $A(\theta)$ , one observes independence on  $\Lambda$  with exponentially increasing accuracy. In the following we shall set

$$\Lambda = \frac{n_\Lambda}{\pi} \text{arccosh} \left( \frac{8 \log 10}{L} \right). \quad (4.1)$$

When  $n_\Lambda = 1$ , we have the exponential factor  $e^{-L \cosh(\pi \Lambda)} = 10^{-8}$  which is a reasonable definition of a *small* quantity in this problem. We shall work with several hundreds of digits which will be enough in all cases where convergence is achieved.

#### 4.1 Ground State

We compared the computation of the ground state energy based on (2.13) or (2.17). The first equation provides much more accurate results and shall be discussed in this section. In the final summary table we shall present results for the second method too. As a preliminary step, we start with  $L = 10^{-1}$  which is the smallest value considered in [11]. We present the time history of the energy iterates at relaxation  $\lambda = \frac{1}{2}$  in Fig. (1). The discretization is  $M = 350$ . One sees that there is easy convergence to a value which has a mild residual dependence on  $\Lambda$ . This dependence can be observed together with the dependence on  $M$  in Fig. (2). A natural simple guess is to assume that for large enough  $\Lambda$  (all considered cases should be all right from this point of view), the relevant parameter is the density of points  $\Lambda/M$ . This hypothesis is tested in Fig. (3). One sees that indeed the dependence on  $\Lambda$  and  $M$  is under control. The considered values of  $\Lambda$  are already asymptotic and the dependence on  $M$  is quite accurately linear<sup>7</sup>. As an interesting additional information, we provide in Fig. (4) the real and imaginary parts of the function  $A(\theta)$ . One sees the initial profile before the iteration loop as well as the final equilibrium value.

The same analysis can be repeated at the very smaller value  $L = 10^{-6}$ . Again, we present the time history of the energy iterates at relaxation  $\lambda = \frac{1}{2}$  in Fig. (5). The discretization is  $M = 500$ . The dependence on  $\Lambda$  and  $M$  is shown in Fig. (6). The scaling plot showing dependence on  $\Lambda/M$  is Fig. (7). Finally, we provide in Fig. (8) the real and imaginary parts of the function  $A(\theta)$ .

This small value of  $L$  permits to emphasize the role of relaxation. This is shown in Fig. (9) where we show the time history of the energy as the relaxation parameter is reduced from 1, where instability is observed, to  $1/3$  where convergence is all right.

#### 4.2 First excited state $\Theta_0$

We present our numerical data for the excited state  $\Theta_0$  following the same scheme as for the ground state. In particular, we show for  $L = 10^{-1}$  the time history of the energy iterates at relaxation  $\lambda = \frac{1}{2}$  in Fig. (10). The discretization is  $M = 350$ . The dependence on  $\Lambda$  and  $M$  is shown in Fig. (11). The scaling plot showing dependence on  $\Lambda/M$  is Fig. (12). Similar plots for  $L = 10^{-6}$  can be found in Figs. (13, 14, 15)). Finally, we provide in Fig. (16) the real and imaginary parts of the function  $A(\theta)$ .

Again, at  $L = 10^{-6}$ , we can show the role of relaxation. This is shown in Fig. (17) where we show the time history of the energy as the relaxation parameter is reduced from 1, where instability is observed, to  $1/2$  where convergence is all right.

---

<sup>7</sup>In principle one can improve the convolutions by improved numerical integrations. Actually, this would be an incomplete improvement and we have checked that residual linear corrections  $1/M$  do remain.

### 4.3 Excited state $\Theta_{00}$

This is the next-to-lowest excited state, at least for small enough size  $L$ . The relaxation algorithm depends now on two independent parameters:  $\lambda_1$  for the update of the function  $A$  and  $\lambda_2$  for the update of the Bethe root(s). We present in Figs. (18, 19) the time history of the energy of the state  $\Theta_{00}$  as well as that of  $\tilde{\theta}_1$  for  $M = 50$ ,  $n_\Lambda = 2$ , and fixed  $\lambda_1 = 1/2$ . As the second parameter  $\lambda_2$  is reduced, we move from an oscillating regime to a convergent one. The onset of oscillations instead of an exponential instability is compatible with the fact that we are dealing with a two component system.

Next, using the parameters shown in Tab. (3), we present at  $L = 10^{-6}$  similar plots to those that we have discussed for the other states. In particular, with discretization  $M = 600$ , we show the dependence on  $\Lambda$  and  $M$  in Fig. (20), the scaling plot in Fig. (21), and in Fig. (22) the real and imaginary parts of the function  $A(\theta)$ .

Finally, in Fig. (23) we show the profile of  $A(\theta)$  which is obtained after convergence at various sizes  $L$ . These could help, at least in principle, in the formulation of suitable proposals for the analytic size dependence of this important function.

### 4.4 Summary tables and $L \rightarrow 0$ limit

Our final results, obtained after extrapolating to  $M \rightarrow \infty$ , are summarized in three tables. For the ground state, they are shown in Tab. (1). The first column reports the results obtained with the TBA NLIE of [7] down to  $L = 10^{-6}$ . The next column shows the results obtained using the equation (2.17). Finally, the third column shows the results which we obtain using Eq. (2.13) which turns out to be much more efficient and accurate. The Y-system results have been obtained reducing the size by two orders of magnitude compared with [7]. The similar Tab. (2) presents our results for the energy of the state  $\Theta_0$  while we present in Tab. (3) the energy of  $\Theta_{00}$  for which there are no available results obtained with other methods.

One can check that there is a very good agreement showing that the GKV equations are working perfectly in the very small size limit. A better precision could be achieved by simply increasing  $M$  in order to reduce the effect of the subleading correction. To the aim of testing the GKV equations, we honestly believe that the quality of our result is convincing.

In Fig. (24), we show the plot of the three energies as functions of  $L$ . The mass gap is clearly reproduced given the agreement between Tab. (1) and the analysis of [7]. There is an additional check that we can perform on our data, and that follows the analysis of [11]. Indeed, all the three considered energies should have the limit  $\frac{L}{2\pi} E \rightarrow -1/4$  as  $L \rightarrow 0$ . This limit is definitely out of reach for the numerics of [11]. Fitting our numbers in the range  $10^{-8} \leq L \leq 10^{-5}$  by means of a (naive) quadratic polynomial in  $1/\log L$  we obtain the three estimates

$$\text{ground state} : -0.249(3), \quad \Theta_0 : -0.2477(1), \quad \Theta_{00} : -0.2439(3). \quad (4.2)$$

These extrapolations are rather close to the predicted limit  $-0.25$ . The quoted errors are simply those inherited from the data. There is no attempt to estimate the systematic error due to subleading corrections in  $L \rightarrow 0$  which are apparently larger for the excited states.

$L$	$E_0$ (NLIE) [7]	$E_0$ (Y-System) Eq. (2.17)	$E_0$ (Y-System)	Parameters
$10^{-1}$	-11.273364587(1)	-11.273(1)	-11.2734(2)	$M = 200 - 350, \lambda = 1/2$
$10^{-2}$	-127.22634373(1)	-127.22(8)	-127.226(2)	$M = 250 - 400, \lambda = 1/2$
$10^{-3}$	-1343.4090793(1)	-1343(3)	-1343.46(2)	$M = 300 - 450, \lambda = 1/2$
$10^{-4}$	-13865.238816(1)	$-1.386(4) \times 10^4$	-13865.8(2)	$M = 350 - 500, \lambda = 1/2$
$10^{-5}$	-141563.8217(1)	$-1.415(5) \times 10^5$	-141564(5)	$M = 350 - 500, \lambda = 1/10$
$10^{-6}$	-1436683.423(1)	$-1.434(7) \times 10^6$	$-1.4367(1) \times 10^6$	$M = 350 - 500, \lambda = 1/10$
$10^{-7}$			$-1.4526(2) \times 10^7$	$M = 350 - 500, \lambda = 1/15$
$10^{-8}$			$-1.4651(4) \times 10^8$	$M = 350 - 500, \lambda = 1/15$

**Table 1:** Ground states energies. The first column is taken from [7]. The second column reports our best results. The last column shows the range of discretization  $M$  and the relaxation parameter.

$L$	$E(\Theta_0)$ (NLIE) [7]	$E(\Theta_0)$ (Y-System)	Parameters
$10^{-1}$	-3.004108884(1)	-3.004109(8)	$M = 200 - 350, \lambda = 1/2$
$10^{-2}$	-69.83802786(1)	-69.8380(3)	$M = 350 - 400, \lambda = 1/2$
$10^{-3}$	-901.2815867(1)	-901.282(9)	$M = 400 - 450, \lambda = 1/2$
$10^{-4}$	-10260.214298(1)	-10260.2(1)	$M = 450 - 500, \lambda = 1/2$
$10^{-5}$	-111091.0324(1)	-111091(2)	$M = 500 - 550, \lambda = 1/2$
$10^{-6}$	-1172575.496(1)	$-1.17258(2) \times 10^6$	$M = 550 - 600, \lambda = 1/2$
$10^{-7}$		$-1.21947(1) \times 10^7$	$M = 550 - 600, \lambda = 1/2$
$10^{-8}$		$-1.25637(1) \times 10^8$	$M = 550 - 600, \lambda = 1/2$

**Table 2:**  $\Theta_0$  energies. The first column is taken from [7]. The second column reports our best results. The last column shows the range of discretization  $M$  and the relaxation parameter.

$L$	$E(\Theta_{00})$ (Y-System)	Parameters
$10^{-1}$	12.423491(8)	$M = 200 - 350, \lambda_1 = 1/2, \lambda_2 = \lambda_1/5$
$10^{-2}$	52.4704(3)	$M = 200 - 350, \lambda_1 = 1/2, \lambda_2 = \lambda_1/5$
$10^{-3}$	123.324(3)	$M = 250 - 400, \lambda_1 = 1/2, \lambda_2 = \lambda_1/5$
$10^{-4}$	-1515.85(2)	$M = 250 - 400, \lambda_1 = 1/2, \lambda_2 = \lambda_1/5$
$10^{-5}$	-35284(1)	$M = 300 - 450, \lambda_1 = 1/2, \lambda_2 = \lambda_1/5$
$10^{-6}$	$-5.0557(1) \times 10^5$	$M = 300 - 450, \lambda_1 = 1/5, \lambda_2 = \lambda_1/10$
$10^{-7}$	$-6.2486(2) \times 10^6$	$M = 200 - 450, \lambda_1 = 1/5, \lambda_2 = \lambda_1/20$
$10^{-8}$	$-7.2033(6) \times 10^7$	$M = 200 - 350, \lambda_1 = 1/5, \lambda_2 = \lambda_1/20$

**Table 3:**  $\Theta_{00}$  energies. The first column reports our best results. The second column shows the range of discretization  $M$  and the relaxation parameters.

## 5. Conclusions

The recent proposal of GKV [11] provides a quite general method to compute finite size

correction to the full spectrum of two dimensional integrable models. It involves non linear integral equations that can be treated in the full space of physical parameters only by means of numerical methods. Whenever integrable discretizations are not available, the calculation of excited levels is based on certain assumptions. For this reason, it is important to compare different methods as well as achieve accurate numerical predictions. In this paper we have worked out the small size limit of the  $SU(2) \times SU(2)$  Principal Chiral Model. To this aim, we have tested a numerical implementation of the NLIE of [11]. We have explored the possibility of solving them by iteration in the case of the ground state and of two additional excited states. We found that small  $L$  values require to introduce relaxation constants in order to achieve convergence. This has to be done independently for the NLIE and Bethe root evolution. We hope that this investigation will be useful in the analysis of the  $SU(N) \times SU(N)$  Principal Chiral Model for general  $N$  along the lines of [12]. We believe that this first steps are necessary in order to attack the full Y-system equations for the AdS/CFT problem [10] having all the systematic errors of the numerics under control.

## References

- [1] J. M. Maldacena, *The Large N limit of superconformal field theories and supergravity*, Adv. Theor. Math. Phys. **2**, 231-252 (1998). [hep-th/9711200].
- [2] See the special issue *Integrability and the AdS/CFT correspondence*, Guest Editors: A. A. Tseytlin, C. Kristjansen, and M. Staudacher, J. Phys. A **A42**, 254002 (2009).
- [3] C. Sieg, A. Torrielli, *Wrapping interactions and the genus expansion of the 2-point function of composite operators*, Nucl. Phys. **B723**, 3-32 (2005). [hep-th/0505071].
- [4] M. Luscher, *Volume Dependence of the Energy Spectrum in Massive Quantum Field Theories. 1. Stable Particle States*, Commun. Math. Phys. **104**, 177 (1986) • M. Luscher, *Volume Dependence of the Energy Spectrum in Massive Quantum Field Theories. 2. Scattering States*, Commun. Math. Phys. **105**, 153-188 (1986).
- [5] C. Destri, H. J. de Vega, *Light Cone Lattices And The Exact Solution Of Chiral Fermion And Sigma Models*, J. Phys. A **A22**, 1329 (1989) • C. Destri, H. J. de Vega, *Integrable Quantum Field Theories And Conformal Field Theories From Lattice Models In The Light Cone Approach*, Phys. Lett. **B201**, 261 (1988) • C. Destri, H. J. de Vega, *Light Cone Lattice Approach To Fermionic Theories In 2-d: The Massive Thirring Model*, Nucl. Phys. **B290**, 363 (1987).
- [6] C. Destri, H. J. de Vega, *Light Cone Lattices And The Exact Solution Of Chiral Fermion And Sigma Models*, J. Phys. A **A22**, 1329 (1989) • A. B. Zamolodchikov, *Thermodynamic Bethe Ansatz In Relativistic Models. Scaling Three State Potts And Lee-Yang Models*, Nucl. Phys. **B342**, 695-720 (1990) • V. V. Bazhanov, S. L. Lukyanov, A. B. Zamolodchikov, *Integrable quantum field theories in finite volume: Excited state energies*, Nucl. Phys. **B489**, 487-531 (1997) [hep-th/9607099] • P. Dorey, R. Tateo, *Excited states by analytic continuation of TBA equations*, Nucl. Phys. **B482**, 639-659 (1996) [hep-th/9607167] • P. Dorey, R. Tateo, *Anharmonic oscillators, the thermodynamic Bethe ansatz, and nonlinear integral equations*, J. Phys. A **A32**, L419-L425 (1999) • [hep-th/9812211]. D. Fioravanti, A. Mariottini, E. Quattrini, and F. Ravanini, *Excited state Destri-De Vega equation for Sine-Gordon and restricted Sine-Gordon models*, Phys. Lett. **B390**, 243-251 (1997) [hep-th/9608091] • V. V. Bazhanov, S. L. Lukyanov,

- A. B. Zamolodchikov, *Integrable structure of conformal field theory, quantum KdV theory and thermodynamic Bethe Ansatz*, Commun. Math. Phys. **177**, 381-398 (1996) [hep-th/9412229] • V. V. Bazhanov, S. L. Lukyanov, A. B. Zamolodchikov, *Integrable structure of conformal field theory. 3. The Yang-Baxter relation* Commun. Math. Phys. **200**, 297-324 (1999) [hep-th/9805008] • J. Teschner, *On the spectrum of the Sinh-Gordon model in finite volume*, Nucl. Phys. **B799**, 403-429 (2008) [hep-th/0702214].
- [7] A. Hegedus, *Nonlinear integral equations for finite volume excited state energies of the  $O(3)$  and  $O(4)$  nonlinear sigma-models*, J. Phys. A **A38**, 5345-5358 (2005). [hep-th/0412125].
- [8] J. Balog, A. Hegedus, *TBA Equations for excited states in the  $O(3)$  and  $O(4)$  nonlinear sigma model*, J. Phys. A **A37**, 1881-1901 (2004). [hep-th/0309009].
- [9] A. B. Zamolodchikov, *TBA equations for integrable perturbed  $SU(2)_k \times SU(2)_1/SU(2)_{k+1}$  coset models*, Nucl. Phys. **B366**, 122-134 (1991) • A. Kuniba, T. Nakanishi, J. Suzuki, *Functional relations in solvable lattice models. 1: Functional relations and representation theory*, Int. J. Mod. Phys. **A9**, 5215-5266 (1994). [hep-th/9309137].
- [10] N. Gromov, V. Kazakov, P. Vieira, *Exact Spectrum of Anomalous Dimensions of Planar  $N=4$  Supersymmetric Yang-Mills Theory*, Phys. Rev. Lett. **103**, 131601 (2009). [arXiv:0901.3753 [hep-th]] • D. Bombardelli, D. Fioravanti, R. Tateo, *Thermodynamic Bethe Ansatz for planar AdS/CFT: A Proposal*, J. Phys. A **A42**, 375401 (2009) [arXiv:0902.3930 [hep-th]] • N. Gromov, V. Kazakov, A. Kozak et al., *Exact Spectrum of Anomalous Dimensions of Planar  $N=4$  Supersymmetric Yang-Mills Theory: TBA and excited states*, Lett. Math. Phys. **91**, 265-287 (2010) [arXiv:0902.4458 [hep-th]] • G. Arutyunov, S. Frolov, *Thermodynamic Bethe Ansatz for the  $AdS_5 \times S^5$  Mirror Model*, JHEP **0905**, 068 (2009) [arXiv:0903.0141 [hep-th]] • N. Gromov, V. Kazakov, P. Vieira, *Exact AdS/CFT spectrum: Konishi dimension at any coupling*, Phys. Rev. Lett. **104** (2010) 211601 [arXiv:0906.4240 [hep-th]].
- [11] N. Gromov, V. Kazakov, P. Vieira, *Finite Volume Spectrum of 2D Field Theories from Hirota Dynamics*, JHEP **0912**, 060 (2009). [arXiv:0812.5091 [hep-th]].
- [12] V. Kazakov, S. Leurent, *Finite Size Spectrum of  $SU(N)$  Principal Chiral Field from Discrete Hirota Dynamics*, [arXiv:1007.1770 [hep-th]].
- [13] J. Balog, A. Hegedus, *TBA equations for the mass gap in the  $O(2r)$  non-linear sigma-models*, Nucl. Phys. **B725**, 531-553 (2005). [hep-th/0504186].
- [14] N. Gromov, V. Kazakov, K. Sakai et al., *Strings as multi-particle states of quantum sigma-models*, Nucl. Phys. **B764**, 15-61 (2007). [hep-th/0603043].
- [15] A. B. Zamolodchikov, A. B. Zamolodchikov, *Factorized S-Matrices in Two-Dimensions as the Exact Solutions of Certain Relativistic Quantum Field Models*, Annals Phys. **120**, 253-291 (1979).
- [16] Paul-Emile Maingé, *Fixed point iterations coupled with relaxation factors and inertial effects*, Nonlinear Analysis: Theory, Methods and Applications **72-2**, 720-733 (2010).
- [17] J. Driesen, R. Belmans, K. Hameyer and J. Fransen, *Adaptive relaxation algorithms for thermo-electromagnetic FEM problems*, IEEE trans. on magnetics, **35-3**, 1622-1625 (1999).

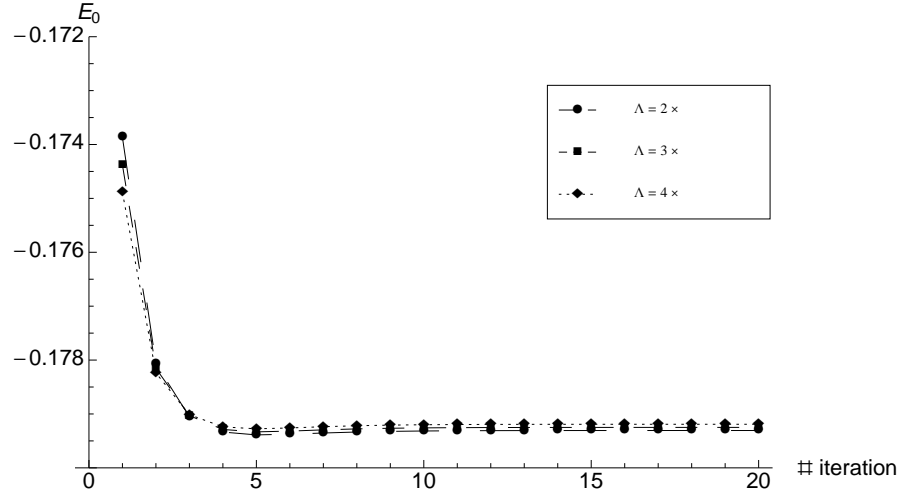


**Figure 1:**  $L = 10^{-1}$ ,  $M = 350$ . Time history of the ground state energy iterates with relaxation  $\lambda = 1/2$ . The notation of the legend is  $\Lambda = n_\Lambda \times \dots$ . The three values of  $n_\Lambda$  are used to check cutoff independence.

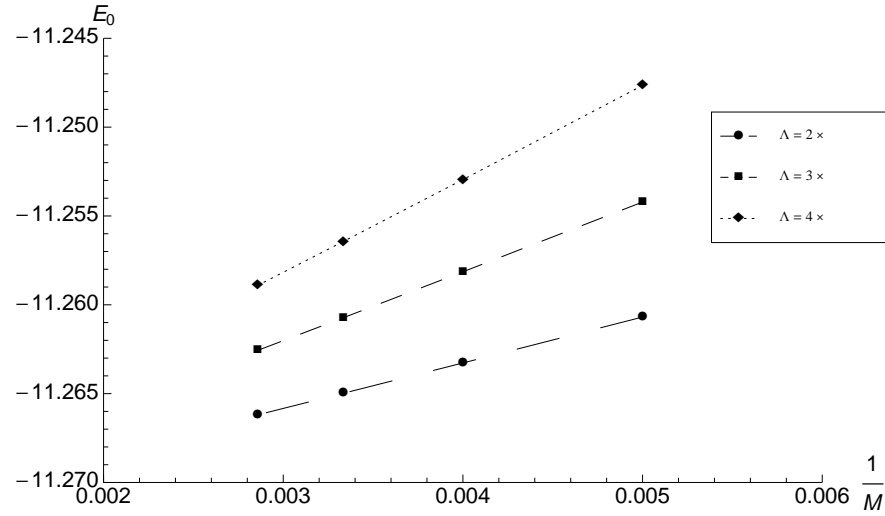


**Figure 2:**  $L = 10^{-1}$ . Ground state energy, after convergence, as a function of  $1/M$ , the discretization roughness, for three values of the cutoff  $\Lambda$ . The notation of the legend is  $\Lambda = n_\Lambda \times \dots$ .



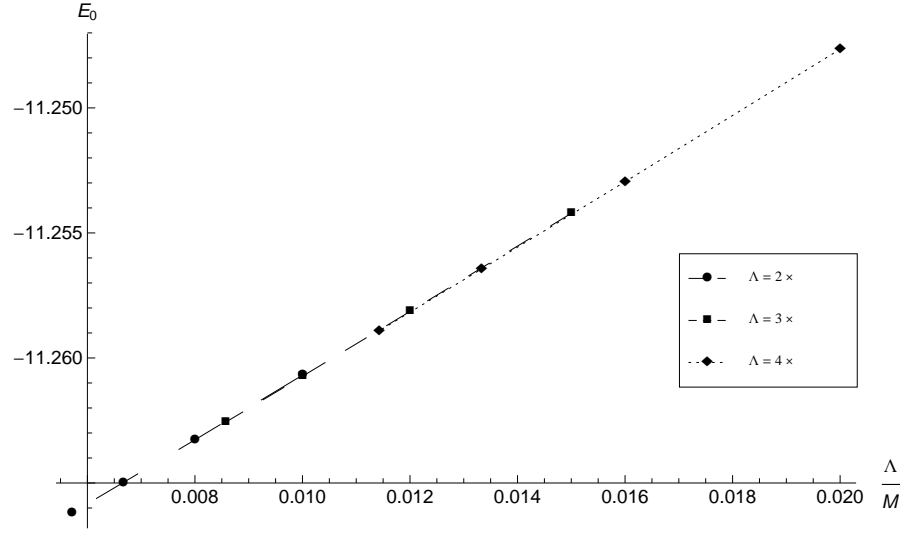


**Figure 3:**  $L = 10^{-1}$ . Ground state energy, after convergence, as a function of  $\Lambda/M$ , the discretization density, for three values of the cutoff  $\Lambda$ . The notation of the legend is  $\Lambda = n_\Lambda \times \dots$ .

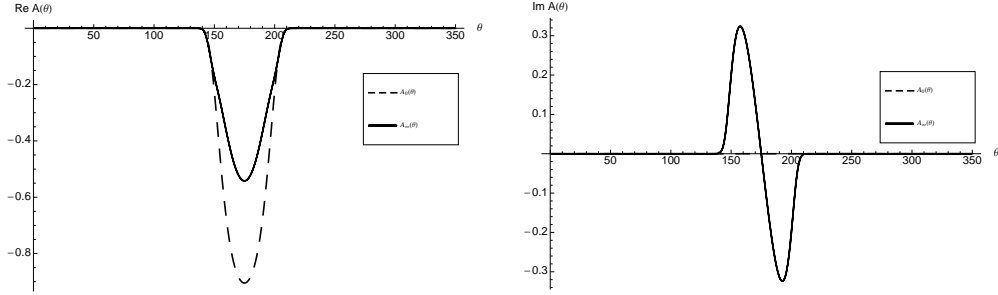


**Figure 4:**  $L = 10^{-1}$ . Profile of  $A(\theta)$  for the ground state, before and after convergence.

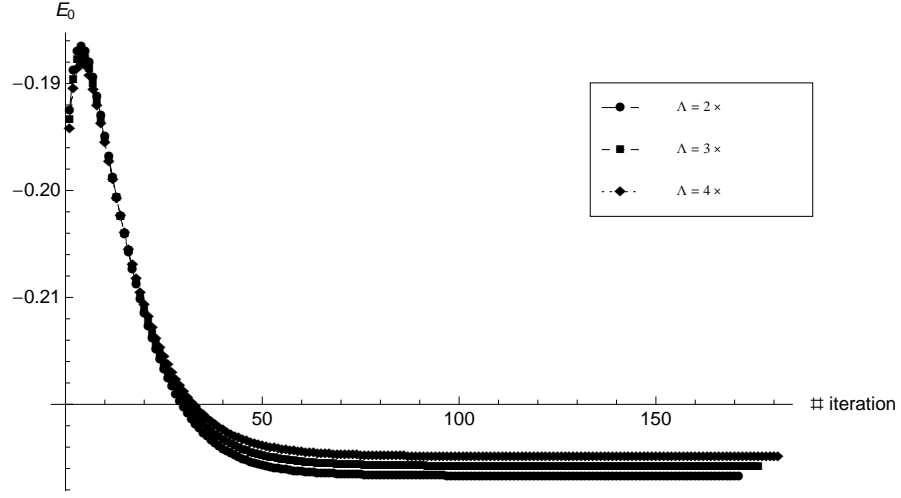


**Figure 5:**  $L = 10^{-6}$ ,  $M = 500$ . Time history of the ground state energy iterates with relaxation  $\lambda = 1/10$ . The notation of the legend is  $\Lambda = n_\Lambda \times \dots$ . The three values of  $n_\Lambda$  are used to check cutoff independence.

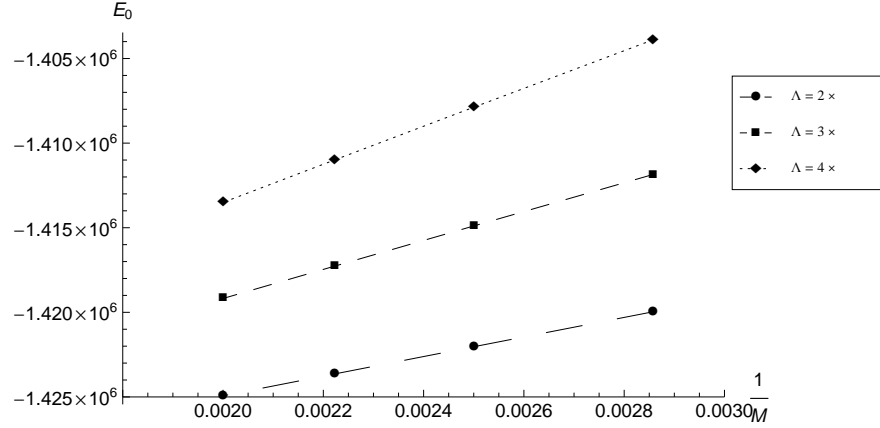


**Figure 6:**  $L = 10^{-6}$ . Ground state energy, after convergence, as a function of  $1/M$ , the discretization roughness, for three values of the cutoff  $\Lambda$ . The notation of the legend is  $\Lambda = n_\Lambda \times \dots$ .

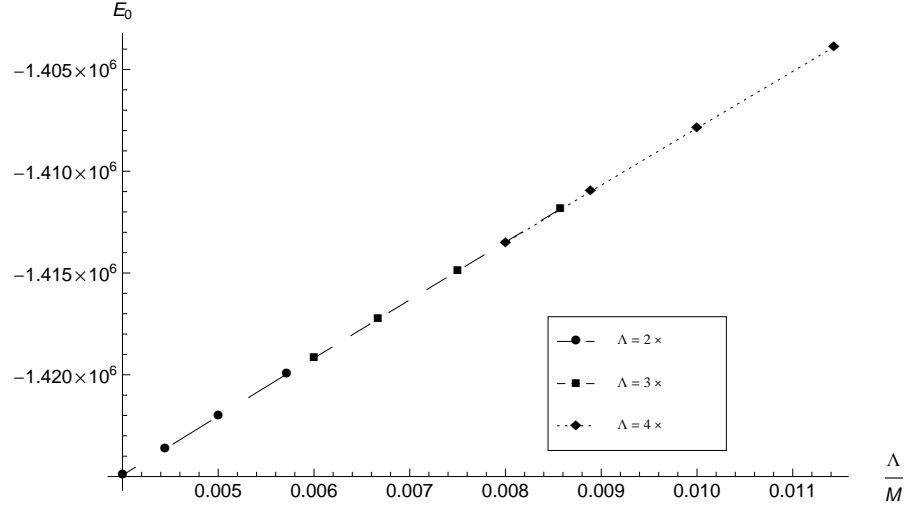


**Figure 7:**  $L = 10^{-6}$ . Ground state energy, after convergence, as a function of  $\Lambda/M$ , the discretization density, for three values of the cutoff  $\Lambda$ . The notation of the legend is  $\Lambda = n_\Lambda \times \dots$ .

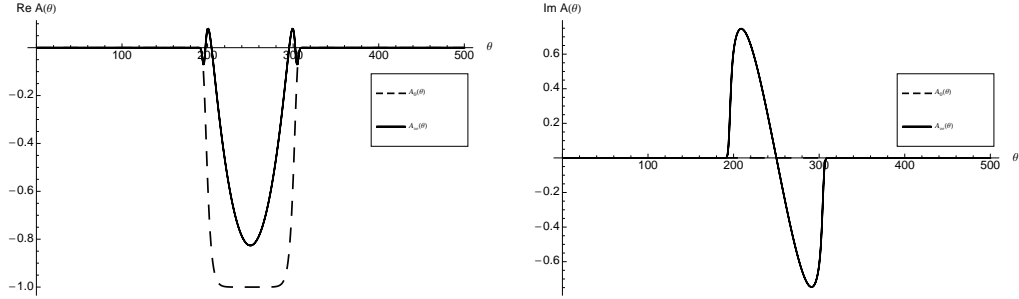


**Figure 8:**  $L = 10^{-6}$ . Profile of  $A(\theta)$  for the ground state, before and after convergence.

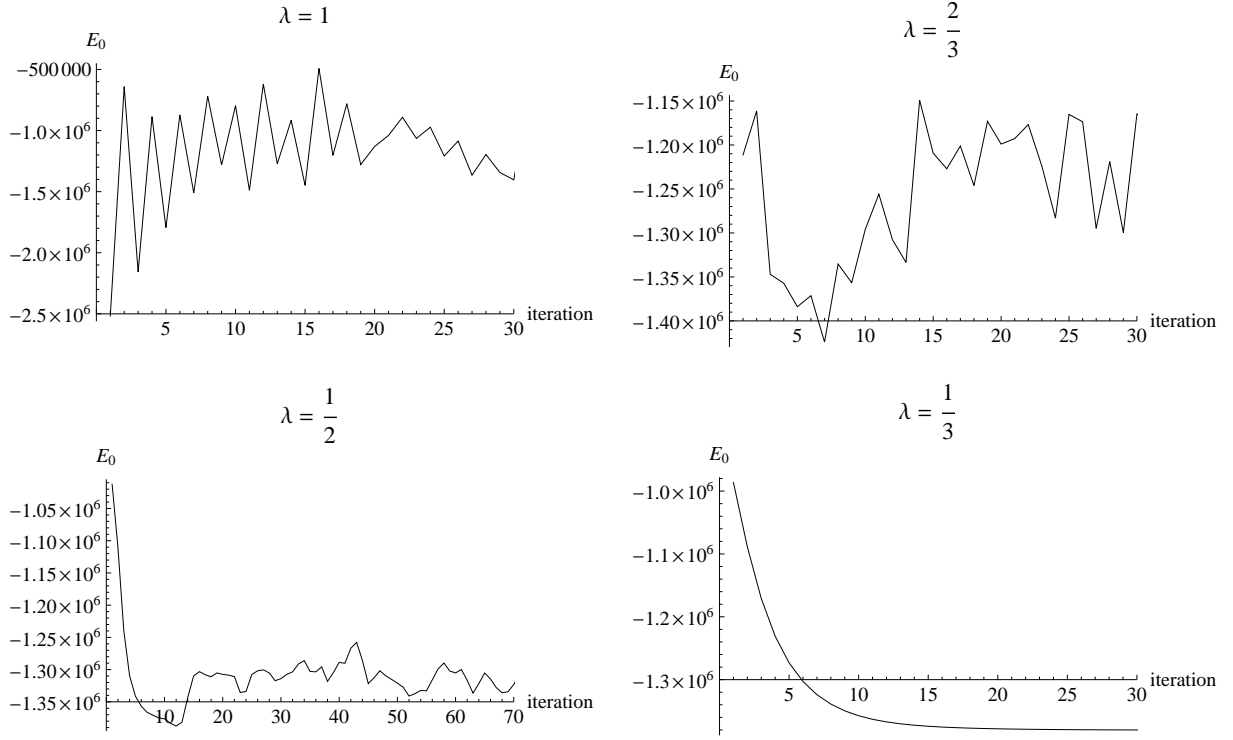


**Figure 9:** Convergence of the energy of the  $\Theta_0$  state at  $L = 10^{-6}$ ,  $M = 100$ , and  $n_\Lambda = 2$ , for various values of the relaxation parameter  $\lambda$ . The computation is done with 250 digits. When the plots start oscillating wildly, convergence is lost and the numerical accuracy rapidly decreases. The plateau which is observed in the first phase of the evolution at  $\lambda = 7/10$  is in agreement with the convergence at  $\lambda = 1/2$ .

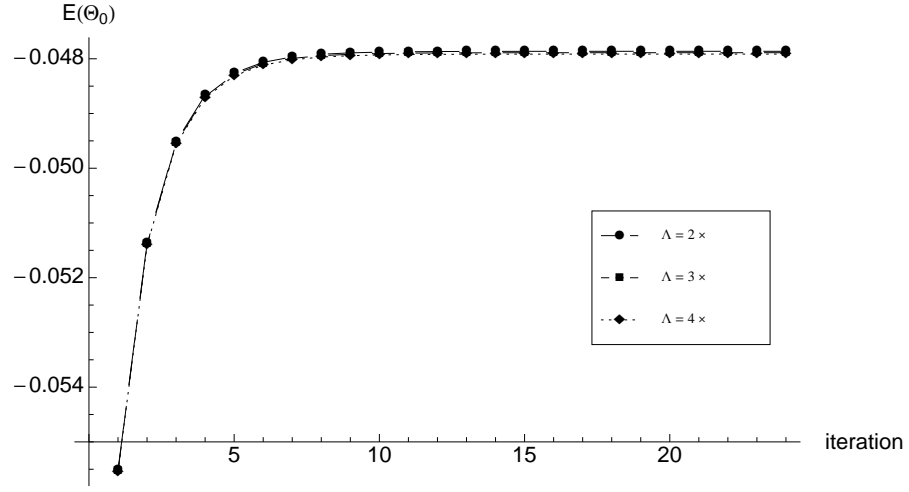


**Figure 10:**  $L = 10^{-1}$ ,  $M = 350$ . Time history of the  $\Theta_0$  state energy iterates with relaxation  $\lambda = 1/2$ . The notation of the legend is  $\Lambda = n_\Lambda \times \dots$ . The three values of  $n_\Lambda$  are used to check cutoff independence.

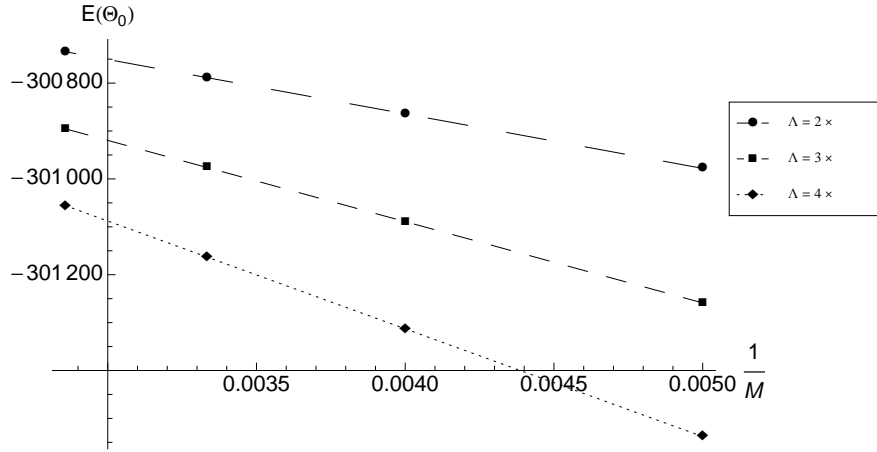


**Figure 11:**  $L = 10^{-1}$ .  $\Theta_0$  state energy, after convergence, as a function of  $1/M$ , the discretization roughness, for three values of the cutoff  $\Lambda$ . The notation of the legend is  $\Lambda = n_\Lambda \times \dots$ .

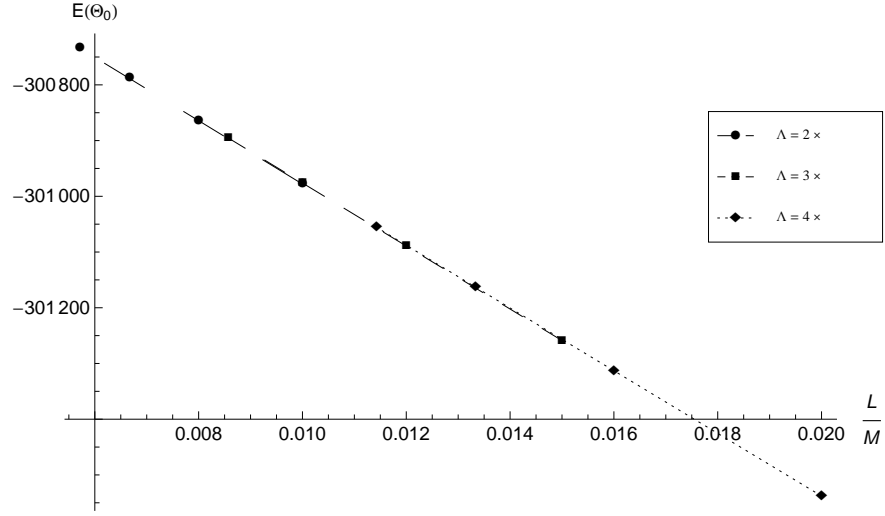


**Figure 12:**  $L = 10^{-1}$ .  $\Theta_0$  state energy, after convergence, as a function of  $\Lambda/M$ , the discretization density, for three values of the cutoff  $\Lambda$ . The notation of the legend is  $\Lambda = n_\Lambda \times \dots$ .

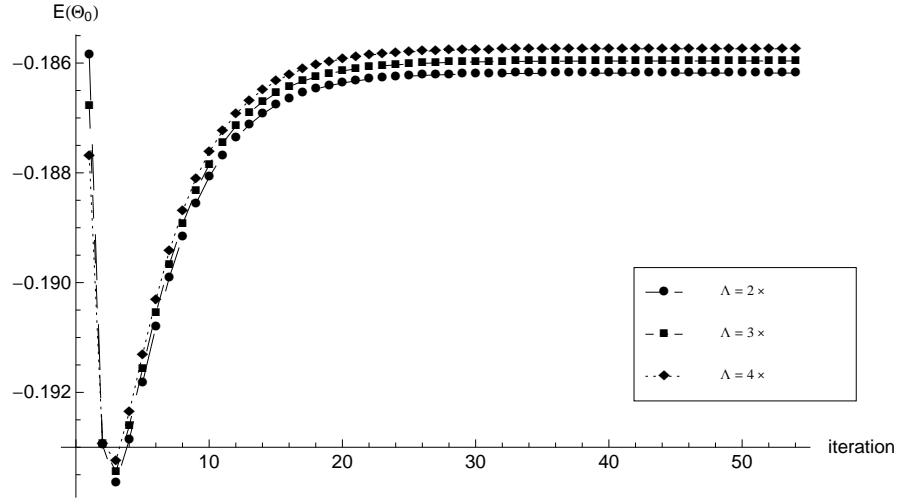


**Figure 13:**  $L = 10^{-6}$ ,  $M = 600$ . Time history of the  $\Theta_0$  state energy iterates with relaxation  $\lambda = 1/2$ . The notation of the legend is  $\Lambda = n_\Lambda \times \dots$ . The three values of  $n_\Lambda$  are used to check cutoff independence.

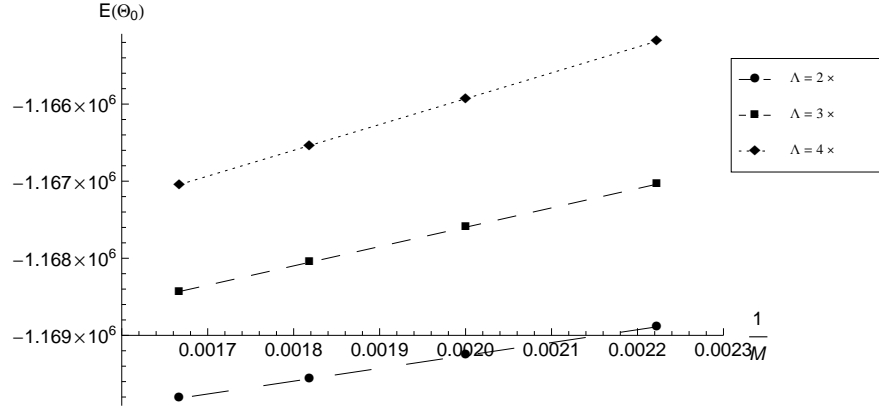


**Figure 14:**  $L = 10^{-6}$ .  $\Theta_0$  state energy, after convergence, as a function of  $1/M$ , the discretization roughness, for three values of the cutoff  $\Lambda$ . The notation of the legend is  $\Lambda = n_\Lambda \times \dots$ .

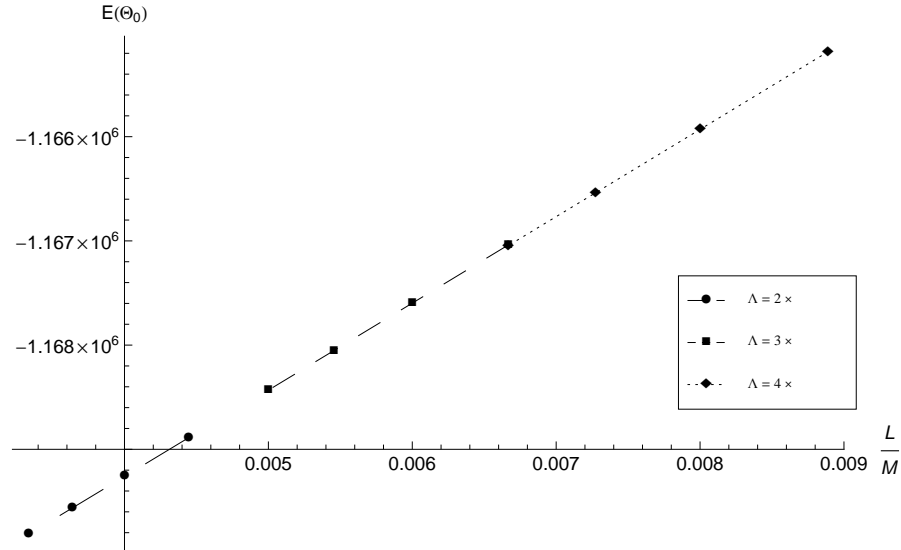


**Figure 15:**  $L = 10^{-6}$ .  $\Theta_0$  state energy, after convergence, as a function of  $\Lambda/M$ , the discretization density, for three values of the cutoff  $\Lambda$ . The notation of the legend is  $\Lambda = n_\Lambda \times \dots$ .

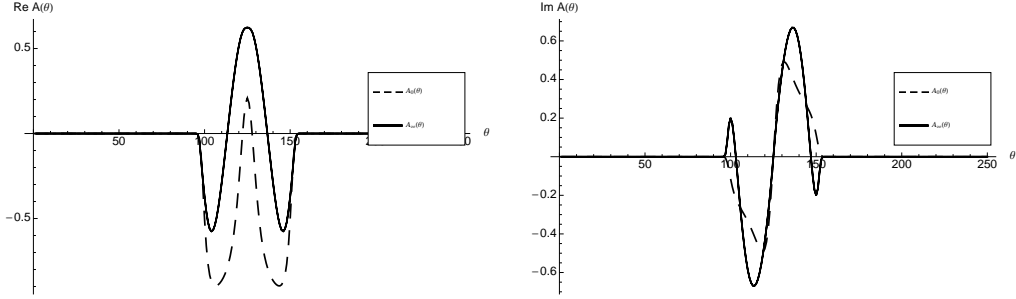


**Figure 16:**  $L = 10^{-6}$ . Profile of  $A(\theta)$  for the  $\Theta_0$  state, before and after convergence.

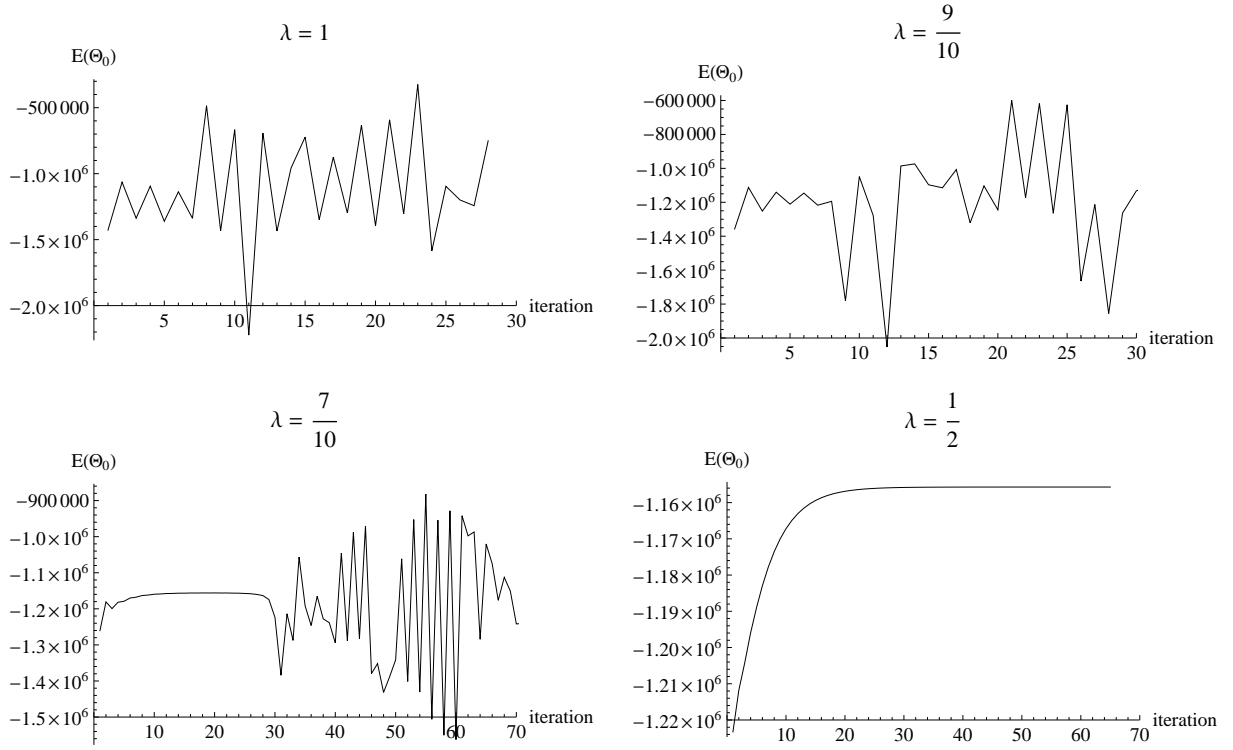


**Figure 17:** Convergence of the energy of the  $\Theta_0$  state at  $L = 10^{-6}$ ,  $M = 100$ , and  $n_\Lambda = 2$ , for various values of the relaxation parameter  $\lambda$ . The computation is done with 250 digits. When the plots start oscillating wildly, convergence is lost and the numerical accuracy rapidly decreases. The plateau which is observed in the first phase of the evolution at  $\lambda = 7/10$  is in agreement with the convergence at  $\lambda = 1/2$ .



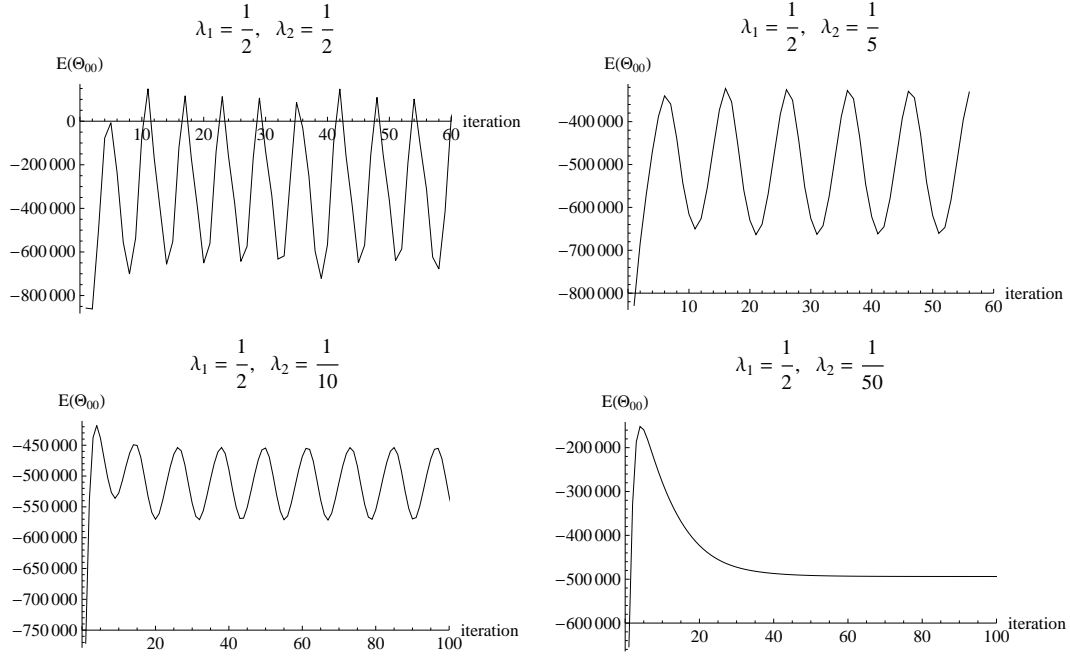


**Figure 18:** Convergence of the energy of the  $\Theta_{00}$  state at  $L = 10^{-6}$ ,  $M = 50$ , and  $n_\Lambda = 2$ , for  $\lambda_1 = \frac{1}{2}$  and various values of the relaxation parameter  $\lambda_2$ .

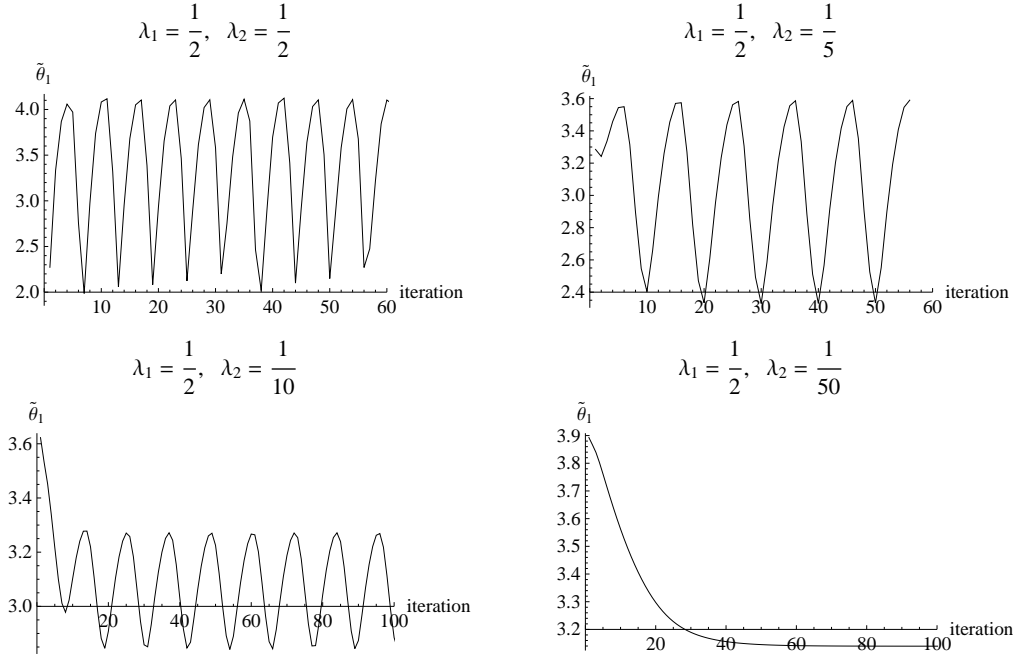


**Figure 19:** Convergence of the Bethe root  $\tilde{\theta}_1$  at  $L = 10^{-6}$ ,  $M = 50$ , and  $n_\Lambda = 2$ , for  $\lambda_1 = \frac{1}{2}$  and various values of the relaxation parameter  $\lambda_2$ .

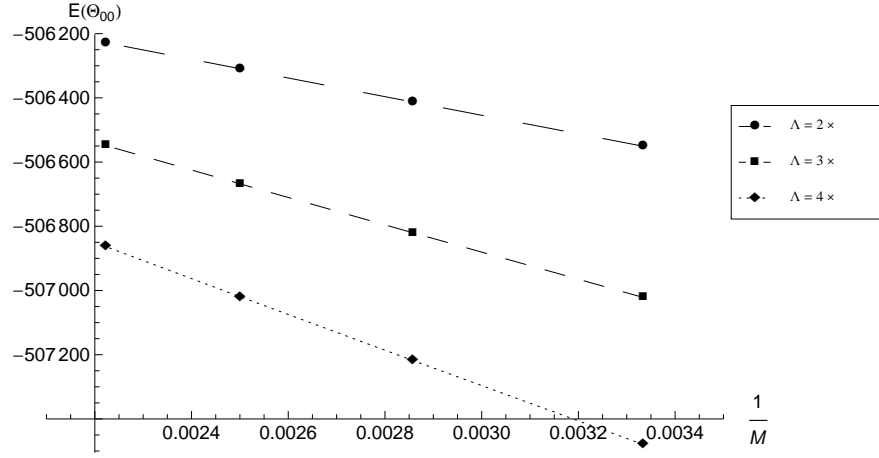


**Figure 20:**  $L = 10^{-6}$ .  $\Theta_{00}$  state energy, after convergence, as a function of  $1/M$ , the discretization roughness, for three values of the cutoff  $\Lambda$ . The notation of the legend is  $\Lambda = n_\Lambda \times \dots$ .

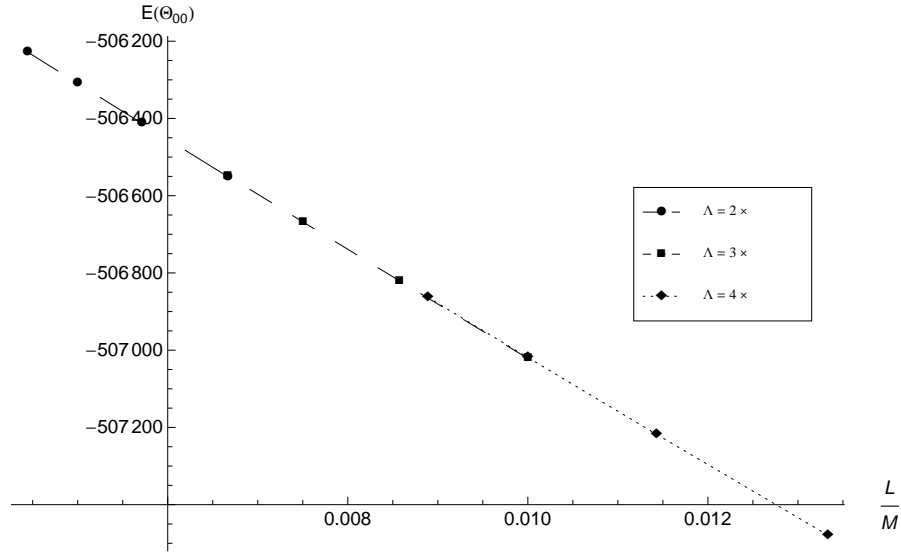


**Figure 21:**  $L = 10^{-6}$ .  $\Theta_{00}$  state energy, after convergence, as a function of  $\Lambda/M$ , the discretization density, for three values of the cutoff  $\Lambda$ . The notation of the legend is  $\Lambda = n_\Lambda \times \dots$ .

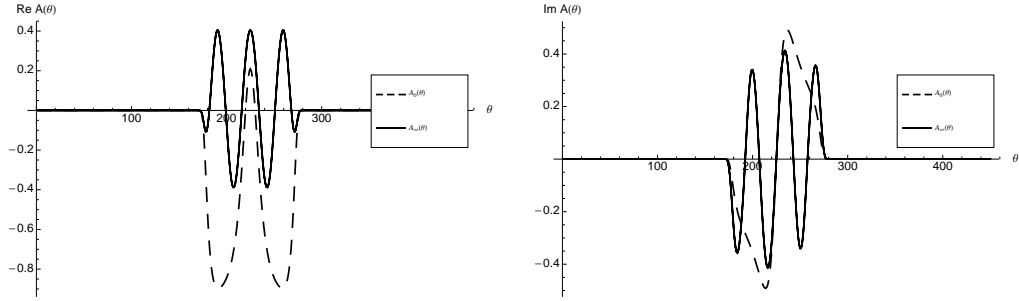


**Figure 22:**  $L = 10^{-6}$ . Profile of  $A(\theta)$  for the  $\Theta_{00}$  state, before and after convergence.

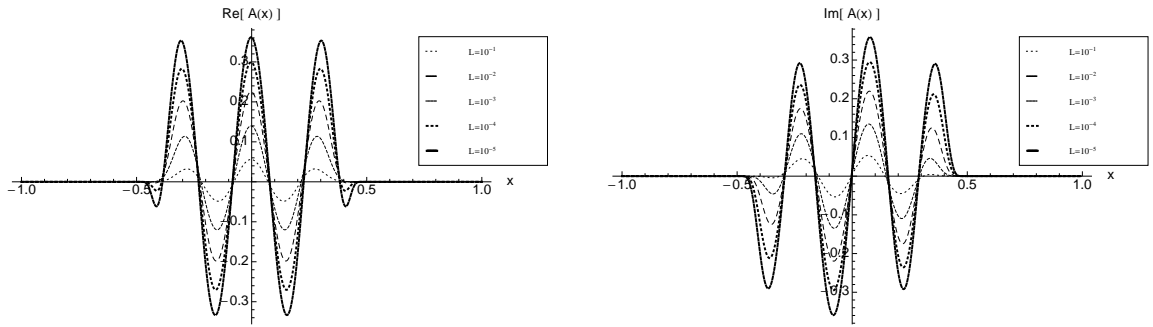


**Figure 23:** Profile of  $A(\theta)$  for the  $\Theta_{00}$  state after convergence at various sizes  $L$ .

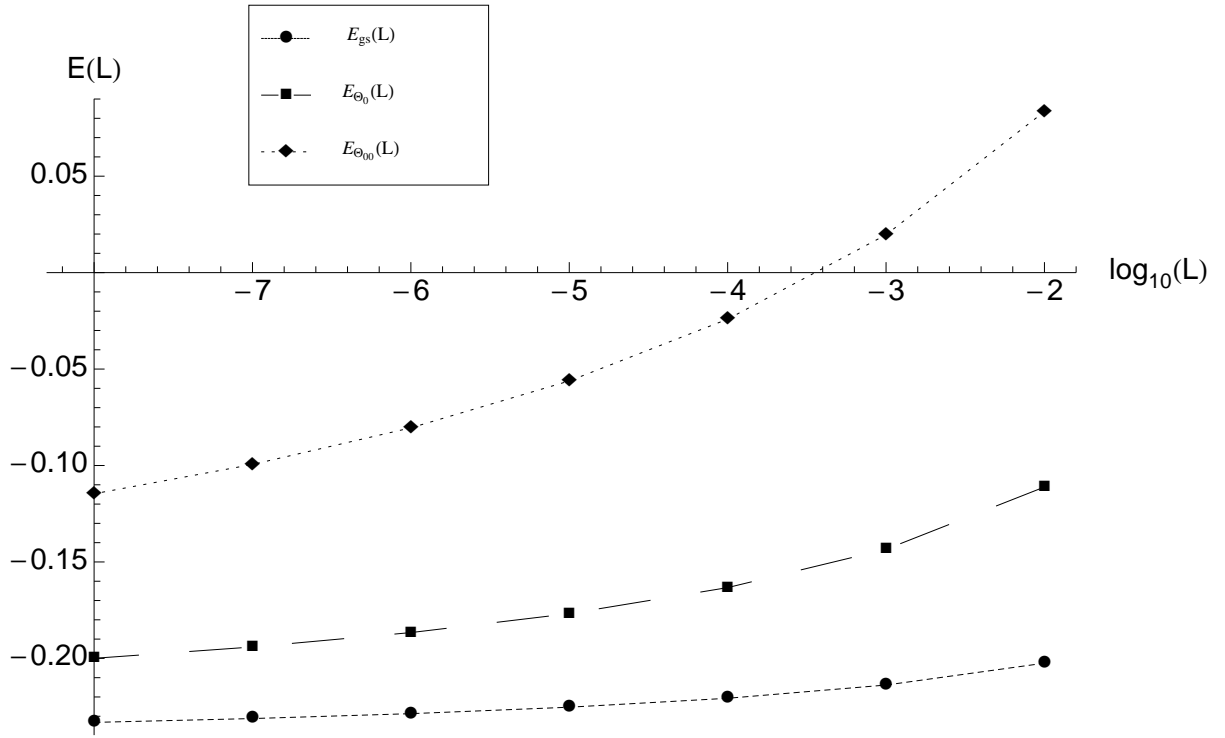


**Figure 24:** Summary plot showing the size dependence of the energies of the three considered states.